T2: Research and development activities on optoelectronic materials and devices at SCLS

Complied by: Dr. V.K.Dixit,
Semiconductor Laser Section
e-mail: dixit@rrcat.gov.in

A summary of the activities of semiconductor laser section (SCLS) is provided in this article. We at SCLS are involved in the research and development of state of the art devices based on semiconductor heterostructures, such as semiconductor laser, detectors etc. For last 15 years, we have been working on metal organic vapour phase epitaxy (MOVPE) growth of semiconductor materials based on group III-V and III-Nitride systems and development of optoelectronic devices. The various activities on experimental and theoretical research being carried out are in the sphere of semiconductor lasers, detectors, nanostructures and spinphotonic.

1. Developmental activities at SCLS

1.a Development of 455 mW/Facet CW Semiconductor diode laser

High power broad area semiconductor lasers emitting at 980 nm wavelength with high electro-optical conversion efficiency, spatial beam quality and reliability have wide range of applications. These laser diodes can be coupled to a multimode fiber and combined to pump Erbium (Er^{3+}) doped fiber amplifiers and configured as high power laser bars to pump solid state lasers for direct material processing applications. We, at SCLS, RRCAT, have already developed high power semiconductor laser with different wavelengths in the range of 0.67 to 1.0 µm with a maximum peak power of 2.5W/facet under pulse mode condition (1:1000 duty cycle). Since then, continuous efforts have been given to increase the output power in CW operation of laser diode for 980nm. Aiming that, we have optimized the MOVPE grown laser structures by parametric studies varying number of QWs, waveguide layer thickness, clad layer thickness and layer doping density. These were aimed at achieving better photon confinement and lower internal resistance of devices for increasing the output power. The MOVPE grown laser structures were processed through conventional optical lithography, n- and p-type contact formation, lift-off process and rapid thermal annealing. The smooth walled MESA structure of laser diode is desired for reducing the scattering loss by surface roughness. The controlled etching of laser structure using H_3PO_4:CH_3OH:H_2O_2 provided a smooth walled MESA structure with surface roughness < 20Å that ensured the surface scattering loss is << 0.1 cm^{-1}. After making a smooth walled MESA structure electrical isolation and side-wall passivation was ensured by SiO_2 layer deposition between the metal electrode stripes. Finally, the structure was thinned down to 120 µm and 1 mm long laser devices were cleaved for testing. The light output versus current (L-I) characteristics of processed laser diode is shown in the Fig. T.2.1. The threshold current density of this laser diode while operated under CW mode is < 150 A/cm^2. As can be seen from Fig. T.2.1 the thermal roll over starts dominating above 1.2 A, hence we have not injected current > 1.3 A At this injected current (1.3 A) laser diode gave an output power of 455 mW/facet (Total 910 mW from the device) at 980 nm emission with spectral width < 2nm as shown in Fig. T.2.1 (inset a, b, c of Fig. 1)[1]. The total device resistance remains within 1.5-2.0 Ω and the dynamic resistance < 75 mΩ during lasing condition. The stability of the laser at about 150 mW/facet (CW) at 0.5 A was within the standard deviation of 5 mW for 10 hours of continuous operation (inset d of Fig. T.2.1). The laser diode characterized above can be further improved after facet coating and bonding of the devices. These steps are already optimized on GaAs wafers and are in the process of being implemented on the laser diode structures.

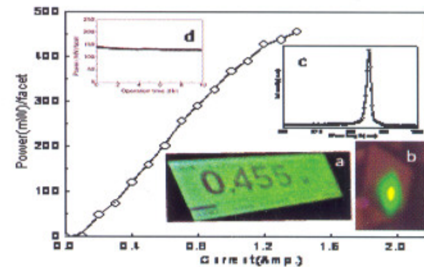

Fig T.2.1 L-I characteristics, inset shows a) Photograph of CW emission on power meter, on b) IR viewer card c) Laser diode spectrum d) Output power versus operation time curve.

1.b Development of semiconductor detectors

1.b.1 Development of GaAs p-i-n detector and effect of γ–ray irradiation on detector parameters:

GaAs based p-i-n devices were processed and irradiation to ^{60}Co γ-ray and effects of irradiation on these devices were determined using temperature dependent current-voltage (I-V) measurements. The ideality factors and series resistance were extracted using curvature function analysis. The series resistance increases with γ-ray irradiation due to the generation of radiation induced defects in the material. The avalanche breakdown voltage increases after irradiation due to decreased mean free path of electron because of increased scattering from generated defects and hence requires large potential to generate electron hole pairs. The peak responsivity 35 mA/W at ~ 650 nm and the radiation hardness value of ~ 4.7x10^{-19}A/cm (Fig. T.2.2) suggests that these devices are good enough to be used in radiation zone below 100 KGy [2].

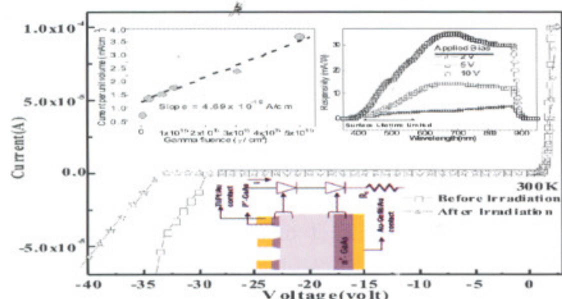

Fig.T.2.2: I-V characteristics of P-I-N diode, Inset shows a)Irradiation effect,b)Response curve, c)P-I-N diode

1.b.2 Quantum well infrared photodetector devices:

Detectors for infrared radiation (IR) are widely used in many applications such as medical, defense and basic sciences. For IR radiation detection HgCdTe (MCT) has been the main material of choice in the past, but due to many problems associated with MCT, III-V based materials have been considered as an alternative. The advantage of making quantum well photodetectors (QWIPs) based on III-V materials such as $Al_xGa_{1-x}As/GaAs$, $In_xGa_{1-x}As/GaAs$ include the mature GaAs growth and processing technologies, which lead to high uniformity, excellent reproducibility, and thus large area and multi colour wavelengths detectivity.

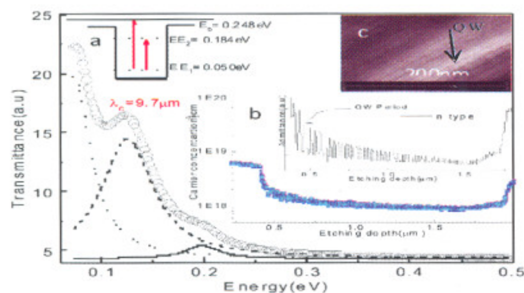

Fig T.2.3.FTIR spectra at 300K ,inset shows a) energy band diagram and transitions correspond to absorption peak b) carrier density profile and admittance variation related to QW period c) Cross sectional bright field TEM image of QWIP structures

We at SCLS, RRCAT have grown 50 period QWIP structures based on $Al_xGa_{1-x}As/GaAs$ QWs using MOVPE. Structural and optical properties evaluated using high resolution x-ray diffraction(HRXRD), transmission electron microscopy (TEM) and photoluminescence (PL) confirms its excellent quality. The carrier density distribution profiles reflect the charge carrier accumulation in the MQWs for all the 50 periods(inset of Fig T.2.3). Fermi energy calculated from the carrier accumulation in the QW satisfies $k_BT < E_f < 2k_BT$ which is the required condition for maximum detectivity of the QWIP. Inter-subband transitions at 9.7 μm (Fig T.2.3) along with low dark current of $Al_xGa_{1-x}As/GaAs$ QWIP MESA devices, suggest their suitability for 8-14 μm range detection [3,4].

1.c Development of indigenous nitride MOVPE reactor

Nitride semiconductors have become an extremely important material system for the fabrication of various optoelectronic and semiconductor devices. MOVPE is one of the most industrially acceptable techniques for the growth of semiconductor materials. Keeping in view the importance of Nitride semiconductors and MOVPE growth process, we at SCLS have developed a Nitride MOVPE system. This system is completely designed and assembled in-house.

The process of Nitride MOVPE involves a high temperature (~above 1000°C) reaction between NH_3 (which is the nitrogen source) and an organometallic chemical like $(CH_3)_3Ga$ via the chemical reaction: $(CH_3)_3Ga + NH_3 \rightarrow GaN + 3CH_4$. Similar reactions between $(CH_3)_3Al$ and NH_3 gives AlN and $(CH_3)_3In$ and NH_3 gives InN. For the growth of ternary materials more than one reaction is carried our simultaneously. The system also has provision to dope the materials n-type with Si and p-type. The heart of the system is the reactor which has a specially designed gas inlet system that allows the vertical injection of the various precursor gases separately inside the reactor with a provision to heat the substrate upto 1200°C. The system, has 32 mass flow controllers, 24 switching valves, a temperature and a pressure controller, all controlled by an indigenously developed SCADA system. Several GaN epilayers have been deposited under different deposition parameters in order to obtain good epitaxial GaN layers. The Fig T.2.4a show the HRXRD rocking curve of the (0002) reflection and the phi scan of the (10-11) reflection to highlight the epitaxial GaN deposited on the sapphire substrates. The 10K PL data of a typical GaN epilayer is shown in Fig T.2.4b.The carrier mobility in grown GaN epilayer is 27 cm^2/Vs with a doping density of ~$10^{19} cm^{-3}$. Efforts are on to improve the quality of grown epilayers.

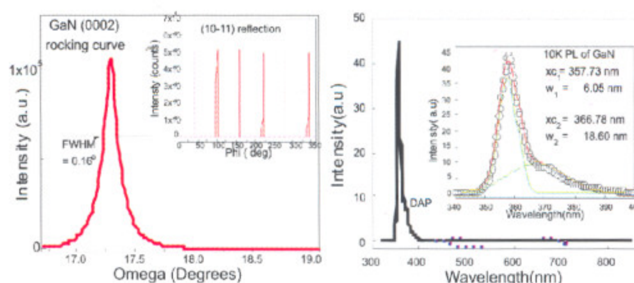

Fig T.2.4. HRXRD pattern and PL spectra confirms good quality GaN epilayers on c-plane sapphire

2. Fundamental studies on InAsP/InP, InP/GaAs, InGaAs/GaAs, GaAsP/AlGaAs QWs and Pt/GaAs, III-V/Si hetrostructures

In addition to $Al_xGa_{1-x}As/GaAs$, other material systems like $In_xGa_{1-x}As/GaAs$, $InAs_xP_{1-x}/InP$ and InP/GaAs (type II), $GaAs_xP_{1-x}/InP$ are grown using MOVPE to explore the possibility of using them for laser, detector and spinphotonic applications.

2.a Composition dependence of the bowing parameter in highly strained InGaAs/GaAs QWs

Highly strained InGaAs/GaAs quantum QWs were studied in-depth using spectroscopic and structural characterization techniques. PL, SPS and PR techniques provided useful information about these QWs at room temperature where PR spectroscopy was found to be the best technique providing sharp and well defined QW features in addition to the GaAs barrier layer signature as shown in Fig. T.2.5. The sharp QW features were then identified by numerically solving the Schrödinger equation for a finite square potential well using the envelope function approximation [5].

The effect of strain in modifying the band structure was also taken into account, including the effect of spin-orbit coupling on the light-hole energy. We were able to identify all the QW features but the indium content required to get a reasonable match was found to be much larger than the value obtained from HRXRD measurements. The systematic HRXRD simulations clearly indicated the absence of any such large error in the QW composition.

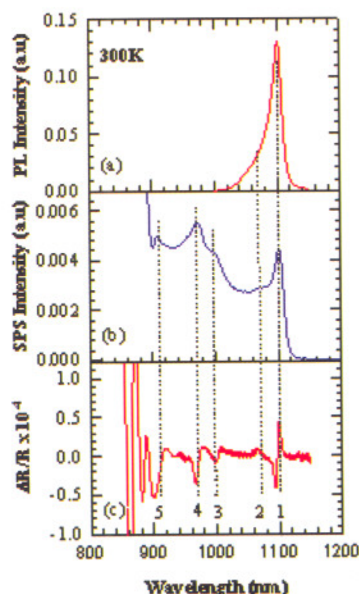

Fig.T.2.5 RT (a) PL, (b) SPS, and (c) PR spectra of f sample A. The vertical dotted lines correlate thee individual components seen in three spectra.

It thereafter led to the discovery of the compositional dependence of bowing parameter for highly strained InGaAs/GaAs QWs where we could identify all the QW transitions by using the QW parameters obtained from HRXRD measurements. It was found that the disorder term 'Ce' of the bowing parameters becomes very important in case of highly strained InGaAs QWs which makes the bowing parameter concentration dependent. It was also found here that the band offset is independent of the composition of InGaAs QWs. We didn't observe any signature of Indium segregation in these QW structures either in spectroscopic or HRXRD characterization because of the low temperature MOVPE growth. The effect of Indium segregation in our samples lies within the error bars defined in HRXRD experiments. Finally, it was also confirmed that the issue of partial relaxation, thought to be very important for highly strained epitaxial layers, seems largely insignificant for this set of InGaAs/GaAs QW samples. It doesn't affect the measured value of bowing parameter for these QW.

2.b Determination of band offsets in InAsP/InP QWs by capacitance voltage profile and photoluminescence spectroscopy

The electron confinement and its transport in $InAs_xP_{1-x}/InP$ QW are determined by the capacitance voltage (C-V) measurements, where the electron accumulation in the QW increases with increasing QWs thickness and arsenic composition. This is due to the effective change in energy level position from Fermi level with the changes of QW layer thickness and arsenic composition (Fig. T.2.6). The conduction band offset (ΔE_c) for $InAs_xP_{1-x}/InP$ QWs has been obtained by solving the self consistent set of Schrodinger and Poisson equations and fitting the theoretical carrier density profile with the apparent carrier density measured from experiments (see the inset of Fig T.2.6). The ΔE_c values are fitted with $\Delta E_c(x) = 402\text{-}350(1\text{-}x)$ meV for $0.38<x<0.62$ and $Q_c=\Delta E_c/\Delta E_g = 0.50\pm0.02$ [6]. These results can be effectively used for designing and evaluating the performance of long wavelength devices

2.c InP/GaAs (type-II) QWs : The type-II band alignment for InP/GaAs heterostructure is studied by means of a novel but simple layer architecture of ultrathin quantum wells (QWs). The cube root dependence of blue shift of the lowest excitonic transition energy on excitation power indicates that the observed luminescence is originating from spatially separated electrons and holes (inset of Fig T.2.7a).

Such a blue shift is seen to increase with the QW thickness again confirming a type-II band alignment. Temperature dependence of the photoluminescence (PL) spectra has been investigated for InP/GaAs type-II ultrathin quantum wells (QWs). Bose–Einstein empirical relation fitting of PL peak energy shows that it follows the temperature dependence of the band gap for InP and/or GaAs materials [7-9]. Thermal escape of carriers from these ultrathin QWs into the barrier is responsible for the PL quenching with temperature. A direct evidence of electron confinement in the conduction band of InP is provided by the C-V analysis.

Quantum states of these QWs are also investigated through temperature dependent C–V measurements. We observe a well-defined peak in the apparent carrier density (ACD) profile for the ultrathin QWs at low temperatures in the vicinity of QWs. ACD peak value is found to decrease with the reduction in QW thickness, indicating quantum confinement effect. Decrease in the ACD peak value and increase in its width with increasing temperature confirms that the observed peak in the ACD profiles is related to the two dimensional electrons occupying the quantum states formed in the ultrathin QWs (Fig T.2.7b). We also determined a strained value of 180±30 meV for the conduction band discontinuity by simulating the C–V profile.

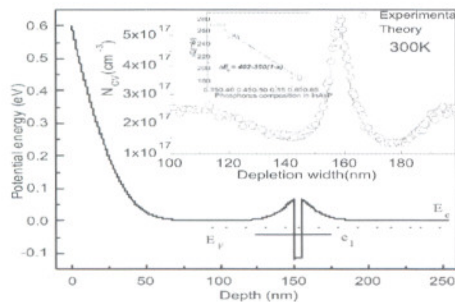

Fig T.2.6. Calculated energy band diagram for the InAsP /InP QW with energy levels. Inset shows ACD profiles and ΔE_c of InAsP/InP QW as a function of composition.

2.d $GaAs_xP_{1-x}/Al_xGa_{1-x}As$ surface quantum well: Surface quantum wells (SQW) have potential applications in high-power surface emitting semiconductor laser and fast quantum well saturable absorber. In such devices, the quantum well QW is placed within a few nanometer of the surface of the device.

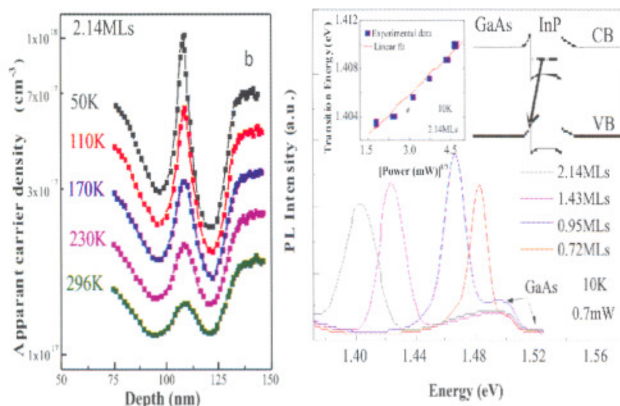

Fig T.2.7. a)10 K PL spectra of ultrathin QWs, inset shows band diagram of InP/GaAs, transition energy vs cube root of the excitation power b) Temperature dependent ACD profile for ultrathin QW.

It is well known that surface states have a detrimental effect on the optical performance of a GaAs based SQW since a high density of surface states pins the Fermi level near the middle of the bandgap. Hence a surface passivation of $GaAs_{0.86}P_{0.14}/Al_{0.6}Ga_{0.4}As$ SQW has been carried out using sulfide solutions for different time durations. The built-in surface electric field is changed via band bending by applying various surface passivation conditions (inset of Fig T.2.8). The band bending is measured using X-ray photoelectron spectroscopy (Fig T.2.8). Reduction in surface electric field in the range of 10-35 kV/cm is observed depending on different passivation conditions. The photoreflectance spectra show enhancement in intensity and blueshift of ~ 3 meV of e1-lh1 transition for SQW passivated with $Na_2S.xH_2O$ solutions for 5 min. Further, blue-shift of 28 meV was observed for same SQW passivated and etched with $Na_2S.\ xH_2O$ solution for 30min. This large blue-shift is attributed to increase in confinement and /or image charge effect due to penetration of the wave function into vacuum [10].

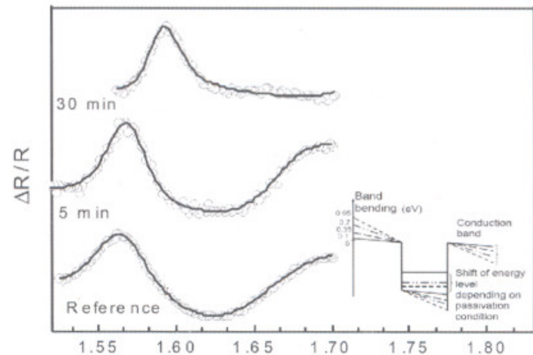

Fig T.2.8. PR of GaAsP/AlGaAs SQW, inset shows the passivation effect on band bending of SQW.

2.e Inverse spin Hall spectra in Pt/GaAs hybrid structure: In recent years, interest in the transport of spin-polarized electrons in semiconductors has been increasing. Intensive experimental and theoretical works have been focused on integrating circular polarized light (CPL) with spinpolarized carriers to develop spin-optoelectronics devices. Recently, an effective and simple method has been demonstrated for detecting light circular polarization based on inverse spin Hall effect (ISHE) in Pt/GaAs hybrid structure (Fig T.2.9a). We are in the process of setting up magneto optical transport measurement facilities at SCLS and during this period we started developing theoretical understandings in some of the issues. In view of this, we have estimated inverse spin Hall spectra using numerical analysis in Pt/GaAs hybrid structure in the range 1–3eV photon energy. The numerical model used here takes account of both energy and spin relaxation phenomena for optically induced hot electrons, tunnelling and thermionic transport effects at Pt/GaAs interface and circular dichroism for the light transmitted through the Pt layer. The

optically excited electrons in GaAs induces a spin current in the Pt layer after crossing the Schottky barrier that leads to transverse electrical voltage due to large spin–orbit coupling in Pt. The magnitude and polarity of this voltage depend on photon energy, angle of incidence of light, and barrier height(Fig T.2.9b). It is found that the magnitude of this voltage is maximum for 60o angle of incidence irrespective of photon energy and barrier height [11].

2.f III-V/Si hetero-structures: The integration of III-V compound semiconductors, which are dominant in applications of optoelectronic devices [12,13], with main stream silicon technology is a very important goal for the semiconductor research and industrial applications. A two-step growth process of GaP, GaAs, InP epilayers on silicon substrate are carried out using MOVPE. This process includes the growth of a low temperature nucleating layer and a high temperature thick epilayer.

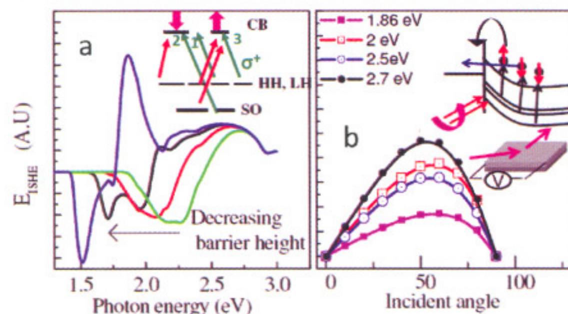

Fig T.2.9.a) EISHE spectra for different Schottky barrier heights, inset shows the inter-band transition in bulk GaAs; red (green) arrows are for left (right) circularly polarized light. b) Magnitude of EISHE as a function of incidence angle for four different excitation energies.

The epilayers of GaP, GaAs, InP grown in two step growth process show significant improvement in morphology compared to that grown by single step process, as confirmed by Raman and SEM studies. HRXRD studies show that the epilayers are of single crystalline nature and structurally coherent with the silicon substrate. Epilayers grown using two-step process show reduced dislocation density and micro-strains, with significant improvements in their structural properties. Furthermore, to evaluate the anti phase domains effect on tilt and twist between the mosaic blocks Williamson-Hall(W-H) analysis is carried out using (002), (004) and (006) reflections. Also for very weak (006) reflection a modified W-H analysis is proposed using (111), (333) and (444) reflections [14]. These results can be effectively utilized for III-V/Si based multi-junction solar cells.

2.g Ab initio studies of GaP Nanoclusters : The semiconductor nanoclusters has been an active area of research over the decades because of their novel properties and various technological applications. Our studies on GaP nanoclusters are directed towards an understanding of the changes in structural and electronic properties of small semiconducting clusters with increasing cluster size, since the nanoclusters are known to exhibit tunable properties which are quite different from those of the bulk material [15]. The calculated optimized structures of Ga_nP_n clusters (n = 2-5) with different possible symmetries are shown in Fig. T.2.10a. We perform full geometry optimization of all GanPn clusters within density functional theory (DFT). All the clusters presented here are stable which has been confirmed by binding energies and harmonic vibrational frequencies analysis and we compare the results with the literature wherever the data available. The results of geometric analysis and binding energy of optimized structures show that the interactions between the atoms in these clusters are weaker than those in the bulk [15].

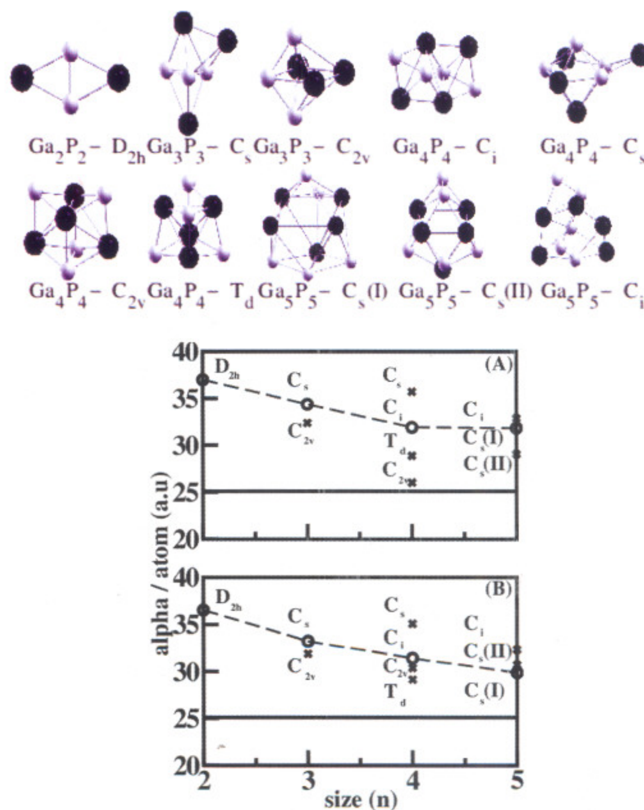

Fig T.2.10. a) Optimizd geometries of Ga_nP_n clusters b) Static polarizability for GanPn clusters from i) MP2, ii)TDDFT method

We calculate the static dipole polarizability of Ga_nP_n clusters by employing various ab initio wave function based methods and DFT/TDDFT method. Our results show that the values of average static polarizability strongly depend on size and symmetry of the clusters. In fig. T.2.10b, we plot the

variation of static mean polarizability per atom with the size of the clusters which has been calculated by MP2 method (top panel) and TDDFT with PBEPBE functional (bottom panel). We observe similar variation of polarizability with the size of the clusters from both the calculations. The circle and the cross in the Fig. T.2.9b represent the values of polarizability for the most stable and other isomers, respectively. The horizontal line represents the value of GaP bulk polarizability per atom. There exists controversy in the literature that whether the values of polarizability reach bulk limit from top or bottom. Our results (in Fig. T.2.10 and on other similar semiconducting cluster) show that the values of polarizability per atom decrease as the size of the clusters increases and reach bulk limit from top (dashed line). This is due to fact that as the size of the clusters increases, system goes from molecular state to solid and hence all the properties of clusters should reach the bulk limit [15]. In smaller clusters the system being smaller in size, they are less compact and have larger polarizability. We also observe that the values of anisotropy in polarizability decrease with the size of clusters. The reason for this is that the clusters become more symmetric as the size of the clusters increases. The optical response properties calculated by us for these systems pave the way to detailed understanding of these and similar materials for device applications.

Reference :

1. "Demonstration of 450 mW/facet CW Semiconductor Laser at 980 nm". V K Dixit, S. Pal, R. Jangir, S. K. Khamari, P. Babudayal, S. D Singh, S. Porwal, R. Kumar, S. Mishra, K. Alexander, T. Ganguli, C. Mukherjee and S. M. Oak, Proceedings of NLS-19, RRCAT, 2010 India.

2. "Effect of ^{60}Co γ-ray irradiation on electrical properties of GaAs epilayer and GaAs p–i–n diode" S. K. Khamari, V.K. Dixit, T. Ganguli, S. Porwal, S. D. Singh, S. Kher, R.K. Sharma, S.M. Oak, Nuclear Instruments and Methods in Physics Research Section B, 269, 272 (2011).

3. "Materials for Infrared Detections: Bulk, Quantum wells, Dots and Dot in Well Structures" V. K. Dixit, S. D. Singh and S. M. Oak, ISSMD, M.S. University, Baroda, Vadodara, 2011, India (Invited).

4. "Studies on GaAs/AlGaAs based (p and n-type) quantum well infrared photodetector structures grown using metal organic vapour phase epitaxy" V. K. Dixit, S. D. Singh, T. K. Sharma, T. Ganguli, S. Pal, B. Q. Khattak and S. M. Oak. IEEE Xplore, 9858874, 355 (2008).

5. "Compositional dependence of the bowing parameter for highly strained InGaAs/GaAs quantum wells", T. K. Sharma, R. Jangir, S. Porwal, R. Kumar, T. Ganguli, M. Zorn, U. Zeimer, F. Bugge, M. Weyers, and S. M. Oak, Phys. Rev. B 80, 165403 (2009).

6. "Determination of band offsets in strained $InAs_xP_{1-x}$/InP quantum well by capacitance voltage profile and photoluminescence spectroscopy", V. K. Dixit, S. D. Singh, S Porwal, R. Kumar, A K Srivastava, T. Ganguli and S. M. Oak, J. of Appl. Phys. 109, 083702 (2011).

7. "Observation of electron confinement in InP/GaAs type-II ultrathin quantum wells", S. D. Singh, V . K. Dixit, S. Porwal, R. Kumar, A. K. Srivastava, T. Ganguli, T. K. Sharma and S. M. Oak, Appl. Phys. Lett., 97, 111912 (2010).

8. "Conduction band offset and Quantum states probed by capacitance-voltage measurements for InP/GaAs type-II ultrathin quantum wells", S. D. Singh, V. K. Dixit, S. Khamari, R. Kumar, A. K. Srivastava, T. Ganguli, and S. M. Oak, J. of Appl. Phys. 109, 073702, (2011).

9. "Temperature dependence of the photoluminescence from InP/GaAs type-II ultrathin quantum wells", S. D Singh, S Porwal, K. Alexander, V. K. Dixit., A. K. Srivastava and S. M. Oak J. Phys. D: Appl. Phys., 43, 455410, (2010).

10. "Comparative study on passivation of $GaAs_{0.86}P_{0.14}$/ $Al_{0.6}Ga_{0.4}As$ near-surface quantum well", S. Pal, S. D. Singh, S. Porwal, S. W. D'Souza, S. R. Barman and S. M. Oak, J. Vac. Sci. Technol. A, 28, 1319, (2010).

11. "Numerical simulation of inverse spin Hall spectra in Pt/GaAs hybrid structure" S. K Khamari, V. K. Dixit and S. M. Oak, J. Phys. D: Appl. Phys., 44, 265104, (2011).

12. "Effect of two step growth process on structural, optical and electrical properties of MOVPE grown GaP/Si". V. K. Dixit, T. Ganguli, T. K. Sharma, S. D Singh, Ravi Kumar, S. Porwal, A. Ingale, P. Tiwari, and S. M. Oak, J. Crystal Growth, 310, 3428 (2008).

13. "Optimization of the properties of MOVPE-grown GaP epitaxial layers on GaP (1 1 1) B substrates, T. K. Sharma, V. K. Dixit, T. Ganguli, S. D. Singh, S. Porwal, R. Kumar and A. K. Nath", Semiconductor Sci and Technol., 23, 075031 (2008).

14. "The study of microstructure of III-V polar on non-polar heterostructures by HRXRD" R. Kumar, T. Ganguli, V. Chouhan and V.K. Dixit, J. Nano- Electron. Phys. 3, 17 (2011).

15. "Ab initio study of stoichiometric gallium phosphide clusters" C. Kamal, T. K. Ghanty, A. Banerjee, A. Chakrabarti, J. Chem. Phys. 130, 024308 (2009).